Kinetics and Catalysis, Vol. 41, No. 6, 2000, pp. 835–843. Translated from Kinetika i Kataliz, Vol. 41, No. 6, 2000, pp. 916–924.

Porous Al_2O_3/Al Metal Ceramics Prepared by the Oxidation of Aluminum Powder under Hydrothermal Conditions Followed by Thermal Dehydration: II. Composition and Microtexture of the Composites

S. F. Tikhov, V. I. Zaikovskii, V. B. Fenelonov, Yu. V. Potapova, V. N. Kolomiichuk, and V. A. Sadykov

Boreskov Institute of Catalysis, Siberian Division, Russian Academy of Sciences, Novosibirsk, 630090 Russia

Received July 26, 1999

Abstract—The microtexture of Al_2O_3/Al composites with different oxide contents formed in the hydrothermal treatment of aluminum followed by thermal decomposition of boehmite is examined by a set of adsorption and structural analysis techniques. Two main types of alumina microtexture are found: relatively loose agglomerates of amorphous particles and highly ordered aggregates of well-crystallized primary blocks of a larger size, the fraction of which increases with the oxide content of the composite leads to an increase in the fraction of micropores and a decrease in the fraction of mesopores. The mechanism of thermal decomposition of boehmite prepared by the hydrothermal oxidation of aluminum is refined.

INTRODUCTION

The macrotexture of porous Al_2O_3/Al metal ceramics prepared by the hydrothermal oxidation of aluminum powder in a closed space followed by the thermal decomposition of boehmite formed was described in the preceding paper [1]. This work was devoted to the study of the microtexture of these composites.

Earlier, studies of this sort have been performed in a free volume. Thus, Yakerson *et al.* [2] examined aluminum oxide prepared by the oxidation of powdered aluminum with water in the presence of indium and gallium additives. They found that the specific surface area of the oxide increases with the concentration of the additives. According to adsorption data, the average pore radius was ~50 Å. Anan'in *et al.* [3] studied the specific surface area of Al_2O_3/Al metal ceramics as a function of temperature of the hydrothermal oxidation; however, the microtexture was not studied in detail. In this work, we analyzed the relationship between the composition and the micropore structure of alumina particles in the same materials on the basis of adsorption and electron microscopy data and the results obtained by small-angle X-ray scattering.

EXPERIMENTAL

The synthesis of samples has been described elsewhere [4, 5]. The specific surface area of all of the samples was determined by a rapid version of the BET method using the thermal desorption of argon. Additionally, the KMT150 and KMT250 samples (Table 1 summarizes the preparation conditions for these samples) were examined in detail on an ASAP-2400 Micromeritics precision instrument using the adsorp-

Table 1. Microtextural characteristics of Al_2O_3/Al composites with minimum and maximum alumina contents, as found from the adsorption–desorption isotherms of nitrogen

Sample	Conditions of preparation	Al_2O_3 content, wt %	Pore volume in the composite, cm^3/g		Specific surface area of the composite, m^2/g			Texture characteristics of Al_2O_3		
			V_s	V_a	S_{BET}	S_Σ	S_{outer}	V_a, cm^3/g	S_Σ, m^2/g	S_{BET}, m^2/g
Parent Al powder	–	~0	0.001	–	0.8	<1.0	–	–	–	–
KMT150	Hydrothermal oxidation (150°C, 0.5 h)	12.2	0.028	0.024	29.1	27.3	3.4	0.21	224	239
KMT250	Hydrothermal oxidation (150°C, 6.5 h)	37.2	0.051	0.044	59.3	57.1	4.0	0.12	154	159

0023-1584/00/4106-0835$25.00 © 2000 MAIK "Nauka / Interperiodica"

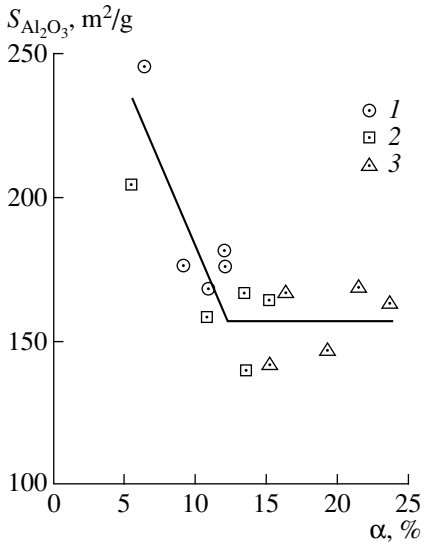

Fig. 1. Specific surface area of Al_2O_3 in Al_2O_3/Al composites as a function of the degree of aluminum conversion in the hydrothermal oxidation reaction performed at temperatures of (*1*) 150, (*2*) 200, and (*3*) 250°C.

tion of nitrogen at 77 K. The adsorption isotherms obtained were used for determining specific surface areas by the BET method (S_{BET}) and for calculating the mesopore distribution and the total volume (V_s) of mesopores filled at the relative pressure $P/P_0 = 0.99$. To analyze the isotherms, a comparative approach [6] was used. This approach is a modification of the Sing α_s-method [7] and other methods based on a comparison between an experimental isotherm and the standard adsorption isotherm obtained in nonporous samples. An adsorption isotherm constructed by averaging the isotherms of nitrogen adsorption on 15 nonporous systems different in chemical nature with specific surface areas up to 1.5 m²/g was used as the standard isotherm [6]. Electron microscopic studies were performed on a JEM-100CX instrument. Conclusions on the crystallographic orientation of pores and particles were drawn on the basis of an analysis of the micrographs and electron-diffraction patterns of differently oriented alumina particles. Small-angle X-ray scattering was examined with a KPM-1 chamber using CuK_α radiation within the angle range from 7′ to 5°.

RESULTS AND DISCUSSION

1. Relationship between the Specific Surface Area of Alumina and the Extent of Aluminum Oxidation

The specific surface area of the two-phase system (S_α) with a developed interface depends on the fractions and specific surface areas of these phases as follows:

$$S_\alpha = S_{Al}(1-y) + S_{Al_2O_3}y, \quad (1)$$

where y is the weight fraction of the oxide in the composite.

The specific surface area of the parent aluminum powder is $S_{Al} \approx 1$ m²/g $\ll S_{Al_2O_3}$, and the values of y and X_0 (relative mass change upon the complete conversion of aluminum into the oxide) can be expressed by the equations

$$y = \frac{\alpha(1+X_0)}{1+\alpha X_0}, \quad (2)$$

$$X_0 = \frac{m_{Al_2O_3}}{m_{Al}} - 1, \quad (3)$$

where α is the conversion of aluminum, and $m_{Al_2O_3}$ and m_{Al} are the masses of alumina (for $\alpha = 1$) and aluminum metal (for $\alpha = 0$) in the composite, respectively. Thus,

$$S_\alpha = \frac{(1-\alpha)S_{Al}}{1+X_0\alpha} + \frac{\alpha(1+X_0)S_{Al_2O_3}}{1+X_0\alpha}. \quad (4)$$

It follows that

$$S_{Al_2O_3} = S_\alpha\frac{(1+\alpha X_0)}{\alpha(1+X_0)} - S_{Al}\frac{(1-\alpha)}{(1+X_0)} \quad (5)$$

or, in view of the above discussion,

$$S_{Al_2O_3} \cong S_\alpha\frac{(1+\alpha X_0)}{\alpha(1+X_0)}. \quad (6)$$

Figure 1 shows the specific surface area of alumina found by Eq. (6) from data on the specific surface area of Al_2O_3/Al metal ceramics of different compositions [4, 5], as a function of the conversion (the degree of hydrothermal oxidation) of aluminum. It can be seen in Fig. 1 that alumina with a higher specific surface area (200–250 m²/g) was formed at the initial stage of the process. The specific surface area became approximately constant (150–160 m²/g) at conversions higher than 10%. Yakerson *et al.* [2] also observed a similar tendency toward a decrease in the specific surface area of samples from ~320 to ~150 m²/g as the conversion of powdered aluminum increased.

2. Micropore and Mesopore Structure of Aluminum Oxide

For a detailed study, we chose composite samples with minimum and maximum alumina contents (Table 1) because these samples were expected to exhibit the most dramatic difference in the texture. Figure 2 shows the adsorption–desorption isotherms for these samples. These isotherms are similar in shape and differ only in the amount adsorbed. The isotherms exhibit typical hysteresis loops in the region of capillary condensation at the relative pressure $P/P_0 \geq 0.40$. The isotherms can be classified by the shape of hysteresis loops as the H2 type according to the IUPAC classification [7]. At the same time, the shape of the hysteresis loop in the isotherm for the parent powdered aluminum is essentially different (this isotherm approaches the H3 type), and

the adsorbed amount is lower by one order of magnitude. This fact suggests that the isotherms for the KMT150 and KMT250 samples are related to only an oxide phase of the composites.

The isotherms given in Fig. 2 are typical of highly porous aggregates with a developed network of intercrossing pores [8]. The linear portion of a desorption branch above the hysteresis loop corresponds to the desorption of nitrogen from a polymolecular adsorption layer at the outer surface of oxide aggregates. The bend (knee) of the isotherm corresponds to the desorption from pores inside aggregated particles. This description is consistent with the comparative adsorption–desorption curves calculated from the isotherms under discussion (Fig. 3). In the region of high pressures, the desorption branch is linear and the outer surface of aggregates (S_{outer}) can be estimated from the slope as 3–4 m^2/g [9]. The total volume of micropores and mesopores within aggregates (V_a) was found by extrapolation of this portion of the comparative curve to the *x*-axis. This volume was greater in the composite with a higher content of oxide, although, if taken with reference to alumina only, the KMT150 sample exhibited a greater volume of micropores and mesopores (Table 1).

The microtextures of the composites were different not only in the volumes of micropores and mesopores. Thus, different segments intercepted the axis of ordinates by extrapolating the linear portions of comparative curves below the bends in the isotherms. For the KMT250 sample, this intercept was several times greater than that for KMT150 (Fig. 3). These intercepts are indicative of the presence of molecule-sized ultramicropores in the samples; the volume of these pores considerably increases with the oxide concentration in the composite. The total volume of these pores in the KMT250 sample is small and equals ~0.005 cm^3/g of the composite; that is, it is lower than 10% of the total pore volume. The presence of ultramicropores is responsible for a disagreement between the total pore volume (V_s) and the volume of micropores and mesopores within aggregates (V_a).

After filling ultramicropores, as the pressure increases, the adsorption occurs on the whole accessible surface of particles that form aggregates (the region below the bend of the isotherm). The slope of the curve in this region of the comparative plot characterizes the total specific surface area (S_Σ), which was higher in KMT250; however, it was higher in KMT150 if referred to alumina (Table 1). These values are close to the specific surface areas of the corresponding aluminum oxides as was measured by the BET method (Fig. 1).

On both of the samples, the adsorption considerably increased at relative pressures lower than those typical of ordinary capillary condensation. This fact can be explained by the mechanism of cooperative adsorption in supermicropores [7]. Adsorption by this mechanism is typical of slot-like pores of width 10–20 Å after the formation of adsorption monolayers on the opposite walls of the pores. The average width of micropores and mesopores was estimated by the equation

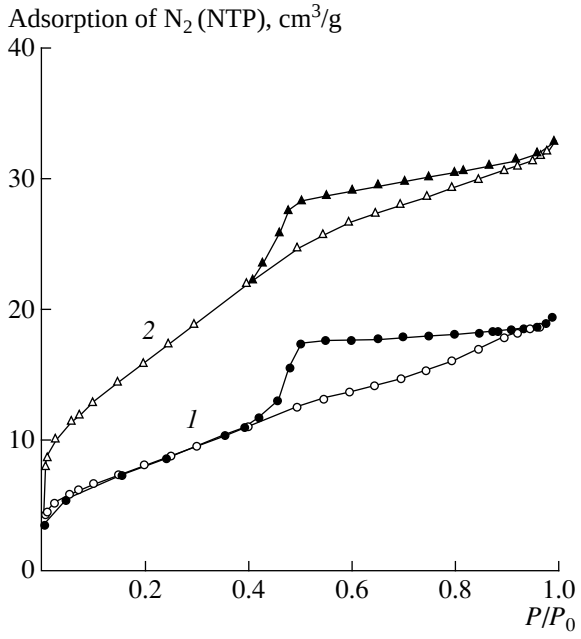

Fig. 2. Adsorption–desorption isotherms of nitrogen at 77 K for the (*1*) KMT150 and (*2*) KMT250 samples (open and closed circles correspond to adsorption and desorption, respectively).

$$h = \frac{2V_\Sigma}{S_\Sigma - S_{outer}}. \quad (7)$$

The values of *h* were equal to ~20 and ~15 Å for KMT150 and KMT250, respectively.

The Broekhoff–de Boer method [10] was used for the analysis of the mesopore structure. According to estimates made using desorption branches of the isotherms, the majority of pores is characterized by a narrow distribution in the region 30–50 Å with a maximum at 34 Å.

A comparison of the alumina samples allowed us to conclude that the texture of KMT150 is looser than that of KMT250; this manifests itself in wider pores and a smaller size of primary oxide particles that form aggregates. Mesopores are more typical of KMT150, whereas micropores and ultramicropores are characteristic of KMT250. It is believed that cermet samples of medium composition (and synthesis conditions) will also exhibit medium texture characteristics as was qualitatively supported by the data of electron microscopy.

3. Microtexture of Aluminum Oxide

For a detailed analysis, we chose three samples synthesized at temperatures of 150, 200, and 250°C. It was

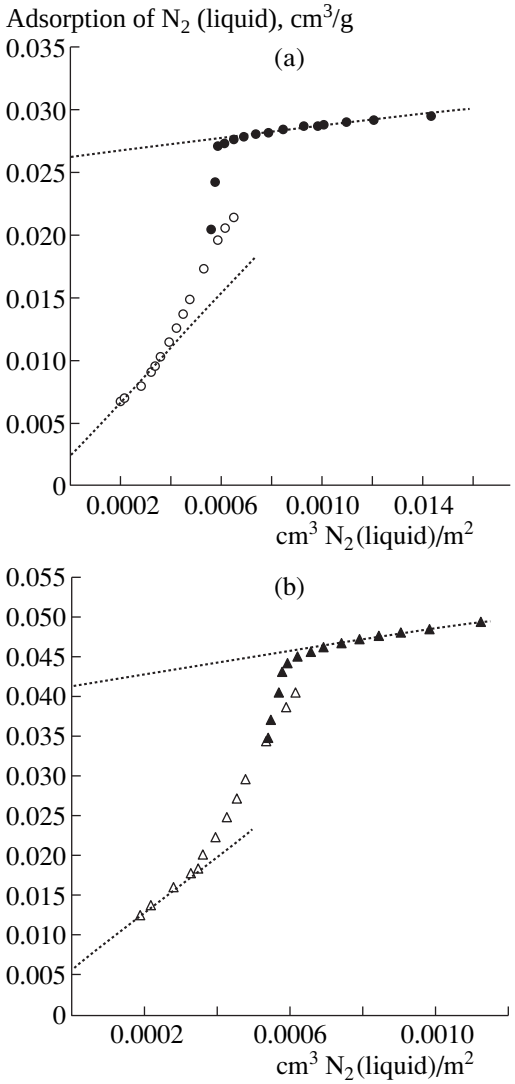

Fig. 3. Adsorption–desorption isotherms of nitrogen (see Fig. 2) plotted in a comparative form: (a) KMT150 and (b) KMT250 (open and closed circles correspond to adsorption and desorption, respectively).

found by scanning electron microscopy that typical aggregates of oxide particles in these samples differ in shape [4].

KMT150 sample (T = 150°C; τ = 0.5 h). Shapeless aggregates that consist of thin twisted fibers 10–20 Å wide and 200 to 800 Å long randomly oriented relative to each other are the most typical of this sample (Fig. 4a). Along with fibers, the aggregates contain primary particles of size 10–20 Å. In a number of cases, plates having slot-like micropores were also observed. The electron microdiffraction patterns of aggregates (see the insert in Fig. 4a) exhibit blurred rings corresponding to a spinel-type structure (interplanar distances d_n = 2.4, 2.0, 1.4 Å, etc.). Other well-crystallized particles were also found, which were more characteristic of samples synthesized at high temperatures of hydrothermal oxidation.

KMT200 sample (T = 200°C; τ = 3.5 h). In this sample, shapeless aggregates similar in morphology to the above were found (Fig. 4b, marked by arrow A). However, the size of primary particles was greater (up to 40–50 Å); this fact is reflected in a decrease in the ring width in the electron microdiffraction patterns (see the insert in Fig. 4b). However, aggregates with an ordered three-dimensional microtexture (they are marked by arrow B in Fig. 4b; see also Fig. 4c) are more typical of this sample. The electron diffraction patterns of these aggregates exhibit a point character; this fact is indicative of high coherence of the crystal lattices of primary blocks on their coalescence into a single crystal. It follows from an analysis of electron microdiffraction patterns that alumina crystals have a spinel-type structure. The substructure of aggregates is produced by plates 70–100 Å in thickness; in turn, the plates consist of primary blocks of size ~40 Å. Micropores ~10 Å in width and up to 50 Å in length are arranged between the primary blocks and plates (Figs. 4c and 4b, marked by arrow B). Thus, these particles exhibit a three-dimensional micropore structure, which includes slot-like pores connected by channels.

KMT250 sample (T = 250°C; τ = 6.5 h). The presence of alumina particles as well-crystallized aggregates of rhombic, hexagonal, and triangular shapes is the most typical of this sample. The particles are up to several micrometers in size and from several hundreds to thousands of angstroms thick. These particles are pseudomorphic to boehmite, which was formed at the stage of hydrothermal treatment. The aggregates consist of plates ~70–100 Å in thickness, which are arranged perpendicular to the [001] direction of a spinel-type cubic lattice and separated by slot-like pores ~10 Å thick (Fig. 4d). Slot-like pores with a similar crystallographic orientation were observed earlier in a sample of γ-Fe_2O_3 prepared by the thermal decomposition of FeOOH in a vacuum [11]. The plates and pores are arranged in an almost ideal order. A disordered layer ~20–30 Å thick (Fig. 4d) was found on one side of the aggregates.

Plates that form an aggregate are discontinuous and consist of blocks from 50 to several hundreds of angstroms in length flattened at the (001) plane. Between the blocks, slot-like pores and channels ~10 Å in thickness were found, the length of which is comparable with the size of primary blocks. The channels are arranged perpendicularly to the planes of plates. A similar pore structure of thin plates of γ-Al_2O_3 prepared from well-crystallized boehmite was observed earlier [12]. The mechanism of thermal decomposition of boehmite is responsible for this structure. Note that the substructures of poorly faceted aggregates typical of the KMT200 sample and of crystalline aggregates of the KMT250 samples are almost identical.

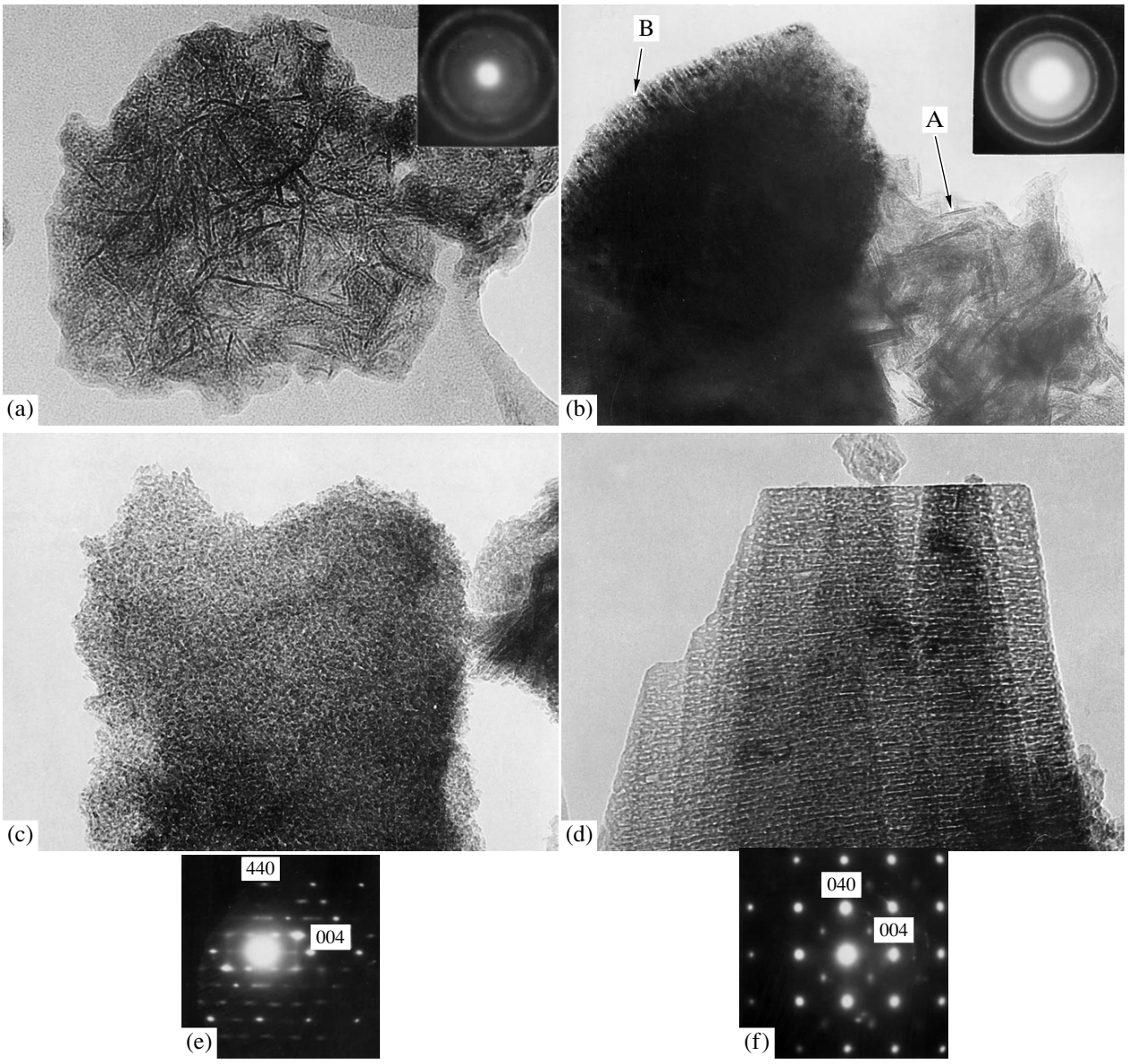

Fig. 4. Electron micrographs of Al_2O_3 particles appearing in various Al_2O_3/Al composites: (a) KMT150 (magnification ×270 000), (b, c) KMT200 (×250 000), and (d) KMT250 (×370 000). Diffraction patterns of oxide zones in the KMT250 sample: (e) zone [110] and (f) zone [100]. The inserts in Figs. 4a and 4b demonstrate the electron microdiffraction patterns of oxide samples.

The point reflections of the [110] zone presented in diffraction patterns (Fig. 4e) confirm the high degrees of crystallinity and mutual order of primary particles that actually form a network crystal. The one-dimensional widening of reflections of the 004 and 440 types results from a very small size of the coherent-scattering region in the [001] direction of the particles and corresponds to packing defects in the structure [13]. On the other hand, reflections of this type in the [100] zone of the diffraction pattern are isotropically widened (Fig. 4f). Thus, we can conclude that packing defects are arranged in the (100) planes.

Note that all of the synthesized samples contained alumina particles of all of the described types. The only difference is in the predominance of a particular type of the most characteristic particles. The aggregates of amorphous particles, fibers, and plates dominate at low conversions of aluminum (KMT150), whereas highly ordered aggregates with developed micropore structures dominate at high conversions of aluminum (KMT250). These highly ordered aggregates are formed by plates in the (001) plane with slot-like channels. In general, with increasing temperature and time of the hydrothermal synthesis, the formed particles of aluminum oxide (hydroxide) undergo changes that are

typical of the aging of aluminum hydroxide, namely, the agglomeration of particles and the formation of well-crystallized aggregates [14]. However, hydroxide particles of all of the morphological types observed in [14] sequentially turned into one another without the retention of previous species. In our case, it is most likely that aluminum oxidation occurs in parallel with the processes of aging of the hydroxides to additionally feed disordered amorphous primary species into the reaction products.

4. Changes in the Size and Concentration of Electron-Density Nonuniformities and the Microtexture of Al_2O_3/Al Composites

It is well known [15] that small-angle X-ray scattering (SAXS) provides data on the size and relative amount of regions with nonuniform electron density, which is different from the electron density of a solid matrix. In our case, at sizes smaller than 300 Å, the integral intensity of nonuniformities increases in proportion to the oxide concentration in a metal–oxide composite (Fig. 5a). An insignificant deviation from zero at a point corresponding to the parent aluminum powder (at a zero conversion) is likely due to a contribution from the oxide film formed upon aluminum oxidation in air. However, the total concentration of nonuniformities in Al_2O_3/Al composites is higher than the concentration in the starting powder by a factor of seven, even at a minimum oxide content (Fig. 5a). Thus, we can conclude that the SAXS data on the electron-density nonuniformities in the composite materials under consideration refer to the oxide phase.

The curve of the size distribution of regions with nonuniform electron density also significantly changed depending on the oxide concentration in the composite (Fig. 6). The parent aluminum powder is characterized by a wide peak with a maximum at 32.5 Å, whereas the maximum for oxide-containing samples is shifted to the region of 18–21 Å. The curves for the KMT200 and KMT250 samples, which are characterized by a high concentration of oxide (long times and high temperatures of the reaction), exhibit an additional maximum in the region 50–55 Å. These results suggest that the size of regions with nonuniform electron density primarily characterizes the average size of primary alumina particles. Indeed, the initial oxide film on the surface of aluminum particles is formed of particles with a characteristic peak at ~32 Å, whereas these particles disappear after the hydrothermal oxidation in the course of which recrystallization of the oxide takes place; this was supported experimentally (Fig. 6). The position of a narrow maximum corresponds to the size of primary oxide particles in the KMT150 sample. The existence of nonuniformities in the region of ~50 Å is due to the appearance of coarser, well-crystallized primary particles in the KMT200 and KMT250 samples; this is evident from electron microscopic data. The fact that this phenomenon is not as pronounced as it would be

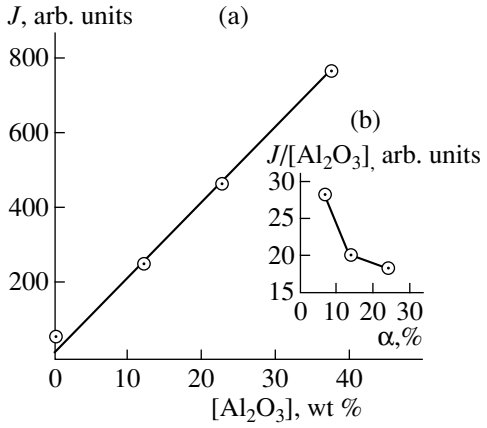

Fig. 5. (a) Concentration of electron-density nonuniformities as a function of the Al_2O_3 content of Al_2O_3/Al composites and (b) concentration of electron-density nonuniformities referred to unit weight of the oxide in the corresponding composites as a function of aluminum conversion.

expected from the electron microscopic data is explained by the formation of packing defects. These packing defects divide the primary blocks into smaller regions with nonuniform electron density. Amorphous particles of a smaller size, which are continuously produced in the oxidation of aluminum, also make this phenomenon less pronounced as described above. Thus, the SAXS data are consistent with the qualitative results of electron microscopic studies and with indirect evidence from the adsorption data that the average size of primary oxide particles increases with conversion (i.e., the extent of aluminum oxidation). At the same time, the SAXS data are also indicative of the possibility of a considerable change in the properties of the oxide itself (its defectiveness) as the reaction occurs and hence of the possibility of a considerable change in the true density, which was found previously [3]. Indeed, the concentration of electron-density nonuniformities per unit weight of the oxide formed in the KMT150 sample (the pycnometric density $\rho_{Al_2O_3}$ = 2.4 g/cm^3) is much higher than that in the KMT200 ($\rho_{Al_2O_3}$ = 3.1 g/cm^3) or KMT250 ($\rho_{Al_2O_3}$ = 3.5 g/cm^3) sample (see Fig. 5b).

5. Micropore and Mesopore Volume of the Oxide and a Mechanism of the Thermal Decomposition of Boehmite Prepared by the Hydrothermal Oxidation of Aluminum

It is well known that the micropore and mesopore structure of γ-Al_2O_3 is formed in the thermal decomposition of boehmite according to the reaction [12]

$$2AlOOH = Al_2O_3 + H_2O\ (+\ pores).$$

To estimate the pore size, data on the specific volumes of boehmite and alumina are required, which are determined from the pycnometric densities. The densi-

ties of the KMT150 and KMT250 alumina samples were published earlier [3]. Table 2 summarizes the pycnometric densities of AlOOH/Al cermets and the densities of boehmite calculated from them. Assuming that the pseudomorphic phase transition is not accompanied by the shrinkage of particles formed (ideal pseudomorphosis), we obtain the following expression for the theoretical pore volume in the thermal decomposition of boehmite [16]:

$$V = (2M_{AlOOH}/(M_{Al_2O_3}\rho_{AlOOH})) - 1/\rho_{Al_2O_3}), \quad (8)$$

where M_{AlOOH} and $M_{Al_2O_3}$ are the molecular weights of the specified phases, and ρ_{AlOOH} and $\rho_{Al_2O_3}$ are the true pycnometric densities of the phases.

The calculated pore volumes are also presented in Table 2. A comparison between these data and the total pore volume (V_s) or the pore volume in aggregates (V_a), which were found from the adsorption data for alumina (Table 1), allowed us to conclude that the experimental values are considerably higher than the calculated data, particularly for the KMT150 sample. Note that a looser product is formed in the thermal decomposition of a looser reagent, because both the water concentration and the theoretical volume of pores produced by the removal of water are similar in the reagent and the product (Table 2), whereas the pycnometric densities of the parent boehmite and the resulting alumina in the KMT150 sample are much lower than those in the KMT250 sample. This fact suggests that the thermal decomposition in both of the samples occurs by about the same mechanisms, which are different from a pseudomorphic transition [12]; this formed the basis for the quantitative estimates in [12, 17]. Indeed, the pseudomorphic mechanism of the thermal decomposition of a layer-like boehmite structure involves opposite migration of aluminum cations and protons to the space between layers of the starting hydroxide. The volume of micropores formed in this manner was estimated [12] at approximately a quarter of the initial volume of boehmite. However, the fraction of the total volume of micropores and mesopores calculated from the adsorption data and referred to the specific volume of boehmite, which was found from the pycnometric density, was ~50 or ~40% of the volume of parent boehmite for the KMT150 or KMT250 sample, respectively. These values are significantly higher than those suggested for the mechanism of an ideal pseudomorphic transition. Thus, the swelling of alumina, which is responsible for a considerable increase in the internal pore volume, occurs in the thermal decomposition of boehmite accompanied by the formation of porous alumina on the surface of aluminum metal.

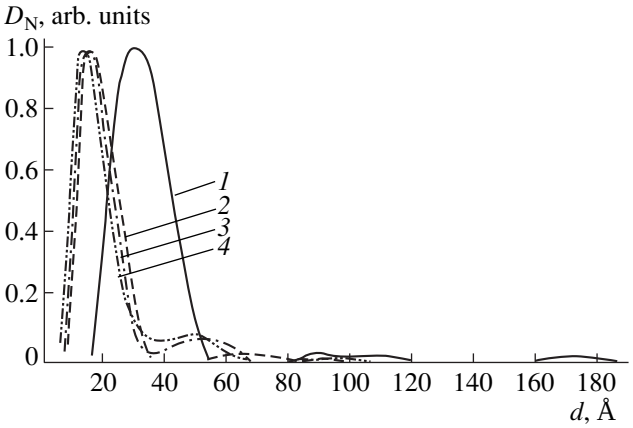

Fig. 6. Size distribution curves for electron-density nonuniformities (according to SAXS data) in (*1*) parent aluminum powder, (*2*) KMT150, (*3*) KMT200, and (*4*) KMT250.

The swelling may result from a disjoining effect, which is not yet completely understood. This effect appears in the dehydration of the most developed (010) planes of boehmite the particles of which are fixed at an end to the surface of aluminum metal. This is the most significant difference between the hydroxide (oxide) formed by hydrothermal oxidation and analogous products prepared by the precipitation method (all particles in these products are less stable, and they easily conglomerate in the course of thermal treatment). Note that, under conditions of boehmite dehydration prepared by hydrothermal oxidation, an exothermic effect is observed at 300–320°C; this effect is not characteristic of boehmite prepared by the aging of coprecipitation products [5]. This is also an indirect evidence for unusual structural and textural properties of the product of hydrothermal oxidation of aluminum. The disjoining effect of products in the dehydration may result from a cooperative process of collapsing a portion of the planes (010) of boehmite. This process is accompanied by the diffusion of protons and hydroxyl groups to the surface of particles. Such a mechanism in the KMT150 sample, in which the particle size of the oxide (and hence the hydroxide) is much smaller, can be considerably facilitated. The appearance of slot-like channels

Table 2. Theoretical estimates of the volume of micropores and mesopores in γ-Al_2O_3 formed by the thermal decomposition of boehmite*

Sample	$\rho_{AlOOH/Al}$, g/cm^3	ρ_{AlOOH}, g/cm^3	$\rho_{Al_2O_3}$, g/cm^3	$V_{Al_2O_3}$, cm^3/g
KMT150	2.71	2.44	2.41	0.067
KMT250	3.01	3.38	3.49	0.062

* The values of $\rho_{AlOOH/Al}$ were found experimentally, and the other were calculated.

perpendicular to the (110) plane of aluminum oxide in the KMT250 sample provides evidence for the existence of a stage of opposite migration of cations and protons. However, by analogy with data in [11], the simultaneous presence of slot-like pores parallel to the (110) plane demonstrates that dehydration also occurs in the topotactic transition of boehmite to the γ-oxide. It is believed that the slot-like channels are formed at the initial stage when the space between the first two (010) planes of boehmite is filled with migrating aluminum cations. Then, the dehydration process takes place with the diffusion of protons and hydroxyl groups to both the edges of particles and the sites where the primary slot-like channels are formed; water can be desorbed through these channels. This mechanism can explain both the formation of highly ordered slot-like pores in the (110) plane of the oxide (as evidenced by the electron microscopic data) and a considerable thickness of oxide plates (40–50 Å), which cannot be attained by simply joining two boehmite planes (~12–15 Å) [12]. Thus, the dehydration of boehmite prepared by the hydrothermal oxidation of aluminum involves processes that occur according to both of the mechanisms, which were opposed previously [12]. This fact can also explain both the presence of slot-like pores and a greater total pore volume than the theoretical value in aluminum oxide.

6. Microtexture of γ-Al_2O_3 Prepared by the Hydrothermal Oxidation of Aluminum

The microtexture of γ-Al_2O_3 prepared by the thermal decomposition of well-crystallized boehmite was also examined previously [18, 19]. The sample prepared by the calcination of boehmite at 580°C exhibited a specific surface area of ~65 m^2/g, and the volume of micropores with a characteristic size of ~11 Å was 0.026 cm^3/g [18]. The samples prepared by the thermal decomposition of boehmite at 450 and 600°C had specific surface areas of 107 and 73 m^2/g, respectively [18]. According to pycnometry data, these samples had a considerable amount of closed pores inaccessible to helium (the volumes of these pores were 0.033 and 0.028 cm^3/g, respectively). However, the total volumes of micropores, mesopores, and closed pores were similar to the theoretical volumes, which were calculated to be equal to 0.121 and 0.114 cm^3/g, respectively, using an equation analogous to Eq. (8). A two-dimensional micropore structure with a characteristic size of ~8 Å of slot-like pores was found by electron microscopy in both of the samples. According to adsorption data, the average micropore and mesopore sizes were 10–15 and 20–40 Å, respectively [19].

In general, the isotherms of nitrogen adsorption on the above samples approach H3-type isotherms, as judged from the shapes of hysteresis loops. Desorption from the outer surface of aggregates was almost absent. The comparative curves of the isotherms of nitrogen adsorption on samples prepared by calcination at different temperatures differed from our plots.

Thus, a decrease in the specific surface area of alumina with conversion can be explained by an increase in the fraction of oxide particles with a greater size of primary particles, which form highly ordered aggregates with a three-dimensional micropore structure. An approximately constant specific surface area results from similar ratios between the particles of different types. A comparison between the oxide obtained by the hydrothermal treatment followed by the thermal decomposition of boehmite and known samples of alumina that was also prepared from boehmite allows us to conclude that a much more narrow size distribution of micropores and mesopores and a greater specific surface area are typical of all Al_2O_3 samples synthesized by the hydrothermal oxidation. In the latter case, the formation of oxide particles with a three-dimensional micropore structure, which are characterized by a higher thermal stability, is primarily responsible for the observed differences.

We compared the data (presented in this work and the preceding paper) on the pore structures of Al_2O_3/Al composite pellets and alumina pellets prepared by the coprecipitation of hydroxides followed by pelletization from a paste-like state [20]. Note that pores of size 50–500 Å were almost entirely absent from the cermet composites with the presence of a considerable fraction of ultramacropores and a developed network of micropores and mesopores, which did not form conglomerates because of the stabilization of highly ordered oxide particles on the surface of aluminum metal.

ACKNOWLEDGMENTS

This work was supported by the Russian Foundation for Basic Research (project no. 99-03-32853).

REFERENCES

1. Tikhov, S.F., Fenelonov, V.B., Sadykov, V.A., *et al.*, *Kinet. Katal.*, 2000, vol. 41, p. 826.
2. Yakerson, V.I., Dykh, Zh.L., Subbotin, A.N., *et al.*, *Kinet. Katal.*, 1995, vol. 36, no. 6, p. 918.
3. Anan'in, V.N., Belyaev, V.V., Romanenkov, V.E., and Trokhimets, A.I., *Vestsi Akad. Navuk BSSR, Ser. Khim.*, 1989, no. 5, p. 17.
4. Tikhov, S.F., Salanov, A.N., Palesskaya, Yu.V., *et al.*, *React. Kinet. Catal. Lett.*, 1998, vol. 64, no. 2, p. 301.
5. Tikhov, S.F., Sadykov, V.A., Potapova, Yu.V., *et al., Stud. Surf. Sci. Catal.*, 1998, vol. 118, p. 797.
6. Karnaukhov, A.P., Fenelonov, V.B., and Gavrilov, V.Yu., *Pure Appl. Chem.*, 1989, vol. 61, no. 6, p. 1913.
7. Gregg, S.J. and Sing, K.S.W., *Adsorption, Surface Area and Porosity*, London: Academic, 1982.
8. Zhdanov, V.P., Fenelonov, V.B., and Efremov, D.K., *J. Colloid Interface Sci.*, 1987, vol. 120, no. 1, p. 218.

9. Fenelonov, V.B., Romannikov, V.N., and Derevyankin, A.Yu., *Micropor. Mesopor. Mater.*, 1999, vol. 28, no. 1, p. 57.
10. Broekhoff, J.C.P. and de Boer, J.H., *J. Catal.*, 1968, vol. 10, no. 4, p. 391.
11. Naomo, H. and Nakai, K., *J. Colloid Interface Sci.*, 1989, vol. 128, no. 1, p. 146.
12. Wilson, S.J., *J. Solid State Chem.*, 1979, vol. 30, no. 2, p. 247.
13. Kryukova, G.N., Zaikovskii, V.I., Plyasova, L.M., *et al.*, *Izv. Sib. Otd. Akad. Nauk SSSR, Ser. Khim. Nauk*, 1984, vol. 3, p. 61.
14. Krivoruchko, O.P., Zolotovskii, B.P., Plyasova, L.M., *et al.*, *React. Kinet. Catal. Lett.*, 1982, vol. 21, p. 103.
15. Kolomiychuk, V.N., *React. Kinet. Catal. Lett.*, 1982, vol. 30, p. 123.
16. Fenelonov, V.B., *React. Kinet. Catal. Lett.*, 1994, vol. 52, p. 367.
17. Tikhov, S.F., Fenelonov, V.B., Zaikovskii, V.I., *et al.*, *Micropor. Mesopor. Mater.*, 1999, vol. 33, p. 137.
18. Lippens, B.C. and Steggerda, J.J., *Physical and Chemical Aspects of Adsorbents and Catalysts*, London: Academic, 1970.
19. Wilson, S.J. and Stacey, M.H., *J. Colloid Interface Sci.*, 1981, vol. 82, no. 2, p. 507.
20. Chertov, V.M., Tsyrina, V.V., and Kaganovskaya, V.A., *Zh. Prikl. Khim.*, 1992, no. 11, p. 2585.